LBL-35943
UC-402
Preprint

Lawrence Berkeley Laboratory
UNIVERSITY OF CALIFORNIA

ENERGY & ENVIRONMENT DIVISION

Submitted to Health Physics

The Influence of a Subslab Gravel Layer and Open Area On Soil-Gas and Radon Entry into Two Experimental Basements

A.L. Robinson and R.G. Sextro

September 1994

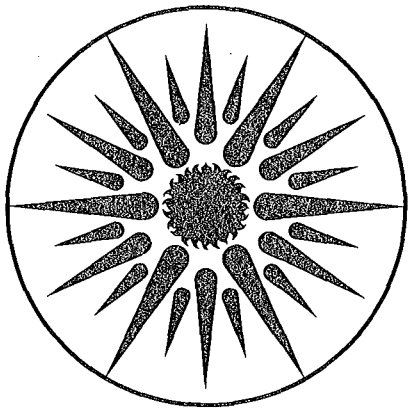

ENERGY & ENVIRONMENT DIVISION

Prepared for the U.S. Department of Energy under Contract Number DE-AC03-76SF00098

To be submitted to *Health Physics*

LBL-35943
UC-402

The Influence of a subslab Gravel Layer and Open Area on Soil-Gas and Radon Entry into Two Experimental Basements

Allen L. Robinson and Richard G. Sextro

September 1994

Indoor Environment program
Energy and Environment Division
Lawrence Berkeley Laboratory
1 Cyclotron Road
Berkeley, CA 94720

This work was supported by the Director, Office of Energy Research , Office of Health and Environmental Research, Environmental Sciences Division, and by the Assistant Secretary for Energy Efficiency and Renewable Energy, Office of Building Technology of The U.S. Department of Energy (DOE), under Contract DE-AC03-763SF00098.

Abstract

Measurements of steady-state soil-gas and ^{222}Rn entry rates into two room-sized, experimental basement structures were made for a range of structure depressurizations (0 - 40 Pa) and open areas (0 - 165 x 10^{-4} m^2). The structures are identical except that in one the floor slab lies directly on native soil whereas in the other the slab lies on a high permeability gravel layer. The subslab gravel layer greatly enhances the soil-gas and radon entry rate into the structure. The radon entry rate into the structure with the subslab gravel layer is four times greater than the entry rate into the structure without the gravel layer with an open area of 165 x 10^{-4} m^2; the ratio increases to 30 for an open area of 5.0 x 10^{-4} m^2. Although open area is a poor indicator of radon and soil-gas entry into the experimental structure, the extension of the soil-gas pressure field created by structure depressurization is a good measure of the radon entry rate into the experimental structures. The measured normalized radon entry rate into *both* structures has the same linear relationship with the average subslab pressure coupling *regardless* of open area. The average subslab pressure coupling is a measure of the extension of the soil-gas pressure field. A three-dimensional finite-difference model correctly predicts the effect of a subslab gravel layer, and different open area configurations on radon and soil-gas entry rate; however, the model underpredicts the absolute entry rates into both structures by a factor of 1.5.

Keywords -- ^{222}Rn, ^{222}Rn entry, soil-gas entry, soil-gas pressure field, soil permeability, numerical modeling

Introduction

Advective flow of radon-laden soil gas is the dominant transport mechanism of radon into houses with elevated indoor radon concentrations (Bruno 1983; Åkerblom et al. 1984; Nero and Nazaroff 1984; Nazaroff et al. 1985; Nazaroff et al. 1988; Turk et al. 1990). Since solid concrete is essentially impermeable to air (Rogers and Nielson 1992), soil gas flows into a basement primarily through cracks, gaps, holes, and other penetrations through the building's foundation. Large gaps are commonly found around plumbing fixtures, utility penetrations, and the perimeter of a floor slab due to the shrinkage gap between the wall and a poured concrete slab. Smaller cracks are created by differential settling of the concrete slab (Scott 1988). A typical basement with concrete wall and floor areas of 120-200 m^2 can have open areas up to a several hundred square centimeters (Scott 1988). Open area is defined as the total cross-sectional area of all penetrations through a foundation. Measurements made in houses in Elliot Lake Ontario indicate that the open area of joints between the walls and the floor slab amount to 0.03 m^2 (Eaton and Scott 1984). In the extreme, cracks with a combined area of 1.5 m^2 were found in a house in New Jersey (Turk et al. 1991a). In addition to flow through cracks, there may also be significant bulk soil-gas flow through basement walls constructed out of a high permeability material such as hollow concrete blocks (Garbesi and Sextro 1989; Ruppersberger 1991).

The importance of cracks as an advective soil-gas entry pathway led to the development of sealing as a radon mitigation technique. However, results from several radon mitigation studies indicate that sealing is often ineffective at reducing indoor radon concentrations (Henschel 1988; Turk et al. 1991a; Turk et al. 1991b). The ineffectiveness of sealing as a mitigation technique was attributed to a failure to seal a significant fraction of the total crack area, and therefore failing to significantly increase the resistance of the foundation to soil-gas flow with respect to the resistance of the soil. Sealing becomes effective when the total substructure crack resistance approaches that of the soil (Mowris and Fisk 1988).

Despite the role of cracks in soil-gas entry into houses and the apparent ineffectiveness of sealing as a radon mitigation technique, little work has been reported on the relationship between open area and soil-gas or radon entry. In a field study, Brennan et al. (1991) found that indoor radon concentrations were independent of changes in open area. They hypothesized that the failure of indoor radon concentrations to increase with increases in open area was caused by elevated soil-gas flow rates diluting the radon concentration of the soil gas. In a modeling study of the influence of different structural factors on radon entry, Revzan et al. (1992) found that radon entry rate was independent of opening width for soils with a permeability less than 10^{-10} m^2, and that the sizes and numbers of openings in the slab were relatively unimportant as long as the total open area is small in comparison to the slab area. That study concluded that the presence of a subslab gravel layer was the most important structural factor considered

with the potential to increase the radon entry rate by as much as a factor of five. Based on the predictions of an analytical model, Mowris (1986) found that cracks wider than 1×10^{-3} m created insignificant resistance to flow in comparison to the resistance of the soil.

This paper reports on a soil-gas and radon entry study carried out at two experimental structures located in the Santa Cruz Mountains, California. These basement structures were designed and constructed to study the importance of structural and environmental factors on radon and soil-gas entry into houses. The two structures are identical except for the presence of a high permeability gravel layer underneath the floor of one of the structures. Inclusion of a subslab gravel layer is a customary construction practice in some areas to provide for water drainage away from the structure, and should conditions warrant, to facilitate radon mitigation (US EPA 1994).

The goals of this work are: 1) to examine the effect of a subslab gravel layer on radon entry rate, 2) to examine the relationship between open area and radon entry rate, and 3) to compare detailed measurements of radon and soil-gas entry with predictions of a three-dimensional finite-difference model. The experiments use constant depressurization of the structure, in the range of 10 to 40 Pa below atmospheric pressure. Open areas are varied by opening and sealing a series of holes and precisely machined slots located in the structure's floor. The results of these experiments can be extrapolated to the few Pascal depressurizations experienced by real houses under ordinary operating conditions because soil-gas flow into the structures is governed by Darcy's law, where flow is a linear function of pressure.

Materials and Methods

Structure Design and Instrumentation

Fig. 1 is a schematic drawing of a basement structure. Each structure is a single chamber with a floor dimension of 2.0 x 3.2 m and a height of 1.9 m (inside dimensions); only about 0.1 m of the walls extend above grade. The structures are identical except for the presence of a 0.1-m-thick gravel layer underneath the slab of one of the structures (Fisk et al. 1992). This structure will be referred to as the gravel structure, and the structure which lies on native soil will be referred to as the no-gravel structure.

A set of slots and holes have been installed in the floor of each structure to provide well-characterized openings through which soil gas flows into the structure. Each structure has six smooth-walled slots to simulate the shrinkage gap that can develop at the floor-wall joint located at the perimeter of poured concrete floors in real houses. Each slot is 3.2×10^{-3} m wide, 0.86 m long and extends though the entire 0.15-m-thick slab. The open area of each slot is 27×10^{-4} m^2. As shown in Fig. 1 the slots are inset 0.34 m from, and run parallel to, each wall of the structures. There are two slots along the east and west

walls, and only one along the shorter north and south walls. These slots provide negligible resistance to soil-gas flow over the range of conditions considered in this study (Fisk et al. 1992). In addition there are four 0.013-m-diameter circular holes drilled in the center of each quadrant of the structure floor. The open area of each hole is 1.3×10^{-4} m^2. There is also a 0.038-m-diameter circular hole in the center of the gravel structure floor, having an open area of 11×10^{-4} m^2. The open area was varied by sealing the various slots and holes in the floor of the structures with aluminum plates and silicone sealant. Great care has been taken to seal all other cracks and other unintended openings between the structure and the soil environment to minimize uncharacterized soil-gas entry points. With all of the openings sealed, only 3.3×10^{-6} m^3 s^{-1} Pa^{-1} of air must be removed from each structure to maintain a constant structure depressurization.

Thirty-two soil probes have been installed around each structure to measure soil-gas pressure disturbances, soil-gas radon concentrations, and soil permeability. As shown in Fig. 1, horizontal probes penetrate the walls at three different elevations, and vertical probes extend through the slab to monitor the subslab region. Table 1 summarizes the distribution and length of the soil probes around both structures. The probes are constructed out of 0.021-m-diameter steel pipe with a 0.15 m section of cylindrical well screen, for sampling, and a 0.04 m driving tip welded onto the end of the pipe (Fisk et al. 1992). A 5-m-long reference probe extends horizontally into the soil from the slab level of the each structure.

Continuous radon monitors (CRM) are used to measure the ^{222}Rn concentration of the air in the structure, slots/holes, and soil. An oscillating fan continually mixes the structure air to allow accurate sampling of structure radon concentration from a single location. Air is drawn from the bottom of all the openings through 0.15-m-long needles, mixed into one sampling line, and delivered to a CRM. Soil-gas samples are multiplexed from the probes to one CRM. The method described by Thomas et al. (1979) was used to interpret the CRM data from the structure and slot CRMs. Since soil-gas samples are multiplexed the algorithm developed by Busigin et al. (1979) was used to interpret the data from the probe CRM (Modera and Bonnefous 1993).

Soil moisture and temperature, indoor and outdoor temperature, wind speed, wind direction, barometric pressure, rainfall, and water table depth are also monitored. A computer-controlled mass flow controller maintains the structure depressurization within $\pm 5\%$ of the set-point. The structure depressurization is the measured pressure difference between the interior and the reference probe. Further details of the design and instrumentation of the structures are found in Fisk et al. (1992) and Garbesi et al. (1993).

Soil Properties

Table 2 reports the measured permeability of the gravel, backfill, and undisturbed soil at the structure site. The permeability of the undisturbed soil is scale dependent, increasing by more than an order of magnitude when the measurement scale increases from 0.1 to 3.5 m (Garbesi 1993; Garbesi et al. 1994). High permeability flow paths such as old plant roots, animal burrows, and water leach pathways are thought to cause the scale dependence of the permeability of the undisturbed soil. The permeability of the undisturbed soil listed in Table 2 is the value measured at the 3 m scale because that is the characteristic length of a soil-gas flow path from the soil surface to an opening in the structure floor. The backfill region, shown in Fig. 1, was excavated during the construction of the structures. It was carefully refilled to minimize the disturbance of the native soil environment (Fisk et al. 1992). The careful packing of the backfill region is thought to have destroyed features which create the scale dependence observed in the undisturbed soil.

Table 3 summarizes measurements of soil-grain density, porosity, emanation fraction and radium content at the structure site. Soil samples were taken from several bore holes, a soil trench, and the walls of the excavations for the structures. Further geological details of the structure site are described in Flexser et al. (1993) and Brimhall et al. (1992).

Pressure Field

The soil-gas pressure field created by depressurization of the interior of the structure drives advective soil-gas entry into the structure. The pressure field quantifies the field of influence of the structure and provides information on the advective soil-gas transport pathways. The soil-gas pressure field is reported in terms of the non-dimensional parameter pressure coupling (Garbesi et al. 1993; Nazaroff et al. 1987). Given Darcy flow and negligible flow resistance though the openings relative to the soil, pressure coupling is independent of structure depressurization.

The pressure coupling at probe j is defined as

$$PC_j = \frac{\Delta P_{ref} - \Delta P_j - \left[\rho(T_{soil}) - \rho(T_{in})\right] g h_j}{\Delta P_{ref}} \qquad 1$$

ΔP_{ref} is the measured pressure difference between the structure interior and the reference probe. ΔP_{ref} is corrected for any pressure coupling in the reference probe by comparing ΔP_{ref} with the time-averaged structure-to-outdoor pressure difference at the soil surface. ΔP_j is the measured pressure difference between the structure interior and probe j. The term $\left[\rho(T_{soil}) - \rho(T_{in})\right] g h_j$ is a small hydrostatic pressure

correction which references PC_j to the slab level. The density (ρ) of the soil gas and the air inside the structure is calculated based on their temperature.

Radon and Soil-gas Entry Rate

Experiments were conducted to determine the steady-state advective radon and soil-gas entry rates into each structure as a function of open area and structure pressurization. Each experiment lasted at least seven days to insure that the structure and soil-gas radon concentrations had achieved steady-state. All of the experiments were conducted during relatively stable environmental conditions -- no large rainfall events, or excessive winds. During each experiment the interior of the structure was held at a constant depressurization relative to the reference probe.

The total advective radon entry rate was computed using a steady-state mass balance

$$S_{adv} = I_{struc} Q_{exh} + I_{struc} \lambda V - S_{diff} \qquad 2$$

where S_{adv} is the total advective radon entry rate into the structure, I_{struc} is the steady-state activity concentration of radon inside of the structure, Q_{exh} is the exhaust flow rate from the structure, λ is the radioactive decay constant of radon (2.1×10^{-6} s^{-1}), V is the volume of air inside the structure (13.4 m^3), and S_{diff} is the diffusive radon entry rate. The measured diffusive radon entry rate through the walls, floor, and openings into both structures, with no imposed structure depressurization, is 0.10 Bq s^{-1} (Garbesi et al. 1993). The diffusive entry rate is assumed to be independent of structure depressurization and open area configuration because the measured soil-gas radon concentration field was relatively invariant during this study.

Although advective radon entry occurs primarily through the slots and holes, it must be corrected for entry through other, non-visible, unintentional openings to make valid comparisons with the numerical model and to study the influence of open area on radon entry. The radon entry rate through the slots and holes (S_c) is calculated by subtracting an estimate of the uncharacterized radon entry rate (S_u) from the total advective radon entry rate:

$$S_c = S_{adv} - S_u. \qquad 3$$

The uncharacterized radon entry rate was estimated by depressurizing the structure with all of the characterized slots and holes sealed and setting S_u equal to the measured total advective radon entry rate. This estimate of S_u represents the upper bound on the uncharacterized radon entry rate. When slots and holes are open, the soil-gas pressure field around the structure changes, reducing the pressure drop across

the structure walls which in turn decreases the flow through any unintentional openings. The uncharacterized radon entry rates are 0.6 Bq s^{-1} and 1.2 Bq s^{-1} at a 20 Pa structure depressurization into the gravel structure and no-gravel structure respectively. In this paper the term "radon entry rate" refers to the advective radon entry rate through the slots and holes, S_c, unless otherwise noted.

After calculating the characterized radon entry rate, the soil-gas entry rate into the structure is determined using a ^{222}Rn mass balance.

$$Q = \frac{S_c}{I_{open}}, \qquad 4$$

where Q is the soil-gas flow rate into the structure through the characterized openings, and I_{open} is the measured ^{222}Rn concentration of the entering soil gas, averaged over all of the openings.

Numerical Modeling

A steady-state, three-dimensional, finite-difference model based on a code written by Loureiro et al. (1990) and modified by Revzan et al. (1992) was used to simulate the soil-gas pressure field around and the advective radon entry into the experimental structures. The model assumes isothermal conditions and Darcy flow. Soil gas flows into the structure through openings defined in the floor of the simulated structure; the rest of the floor and the walls are treated as no-flow boundaries. The model assumes that all openings in the floor provide no resistance to flow of soil gas, i.e. that the openings provide negligible resistance to soil-gas entry in comparison with the soil.

Two types of openings are defined in the floor of the modeled structure: long slots with the same dimensions and locations as the slots in the experimental structures, and square holes with the same area and location as the circular holes in the floor of the experimental structure. The assumption of insignificant pressure drop across openings is valid for all configurations except for the case of the gravel structure with only holes open. In this configuration the flow rate through the openings is high enough to cause some pressure drop in the openings -- on the order of 5% of the total imposed pressure on the structure. Corrections for pressure drop in the holes were made using a correlation developed by Shah (1978) which predicts the pressure drop in the inlet region of non-circular ducts. The flow through the holes is not fully developed because the slab thickness is only 12 times the hole diameter.

To simulate the soil-gas flow field the modeled soil block was divided into three regions: undisturbed soil, backfill, and subslab region (Garbesi 1993). The different soil regions are shown in Fig. 1 and are assigned the measured permeabilities reported in Table 2. The subslab region in the no-gravel structure is assigned the permeability of the undisturbed soil. The modeled soil block was divided into layers to

simulate the soil-gas radon concentration field (Garbesi 1993). The depths and properties assigned to the modeled layers correspond to those listed in Table 3.

Results and Discussion

Soil-Gas Entry as a Function of Structure Depressurization with Six Slots Open

Fig. 2 shows the measured soil-gas entry rate into the gravel and no-gravel structure as a function of structure depressurization. The measured soil-gas entry rate was determined from a radon mass balance. All of the measurements presented in Fig. 2 were made with six slots open, a total open area of 165×10^{-4} m^2. As expected from Darcy's law and the negligible resistance of the slots to flow, the soil-gas entry rate is a linear function of structure depressurization. A linear regression of the soil-gas entry rate as a function of structure depressurization, weighted by the measurement uncertainties, yields slopes of 9.8×10^{-6} m^3 s^{-1} Pa^{-1} ($r^2 = 0.99$) for the gravel structure, and 2.5×10^{-6} m^3 s^{-1} Pa^{-1} ($r^2 = 0.98$) for the no-gravel structure. With all six slots open the measured soil-gas entry rate into the gravel structure is approximately four times greater than the measured soil-gas entry rate into the no-gravel structure. To verify the accuracy of determining the soil-gas entry rate with a radon mass balance, the soil-gas entry rate through the 0.038-m-diameter hole in the gravel structure was calculated with a radon mass balance and directly measured using a hot wire anemometer. The two measurements were less than 5% different -- less than the experimental uncertainty. Fig. 2 shows that the model underpredicts the soil-gas entry rate into both the gravel and no-gravel structure by a factor of 1.5 and 1.4 respectively. Although the discrepancy for the no-gravel structure is slightly smaller than for the gravel structure, this difference falls within the uncertainties of the permeability measurements input into the model and soil-gas entry rate measurements.

Garbesi et al. (1993) reported a soil-gas entry rate into the gravel structure of 1.7×10^{-5} m^3 s^{-1} Pa^{-1}. The apparent reduction in soil-gas entry rate reported in this study is due to improved accuracy in the measurement of the radon concentration of the slot air. In the present study 0.15-m-long needles were used to sample air from the bottom of the slots. In the previous study 0.016-m-long needles were used to sample air from the slots; these shorter needles may have entrained air from the structure, diluting the slot air radon concentrations.

Pressure Coupling with Six Slots Open

Pressure coupling measurements made around both structures with six slots open are presented in Figs. 3, 4, and 5. As expected the pressure coupling decreases as one moves away from the openings. The notable exception is found in the mid-wall of the no-gravel structure, shown in Fig. 5. However,

these small values of pressure coupling have large experimental uncertainties associated with them. The pressure gradient is much larger in the subslab region where the soil-gas flow field converges into the slots (Fig. 3) than around the low and mid-wall probes where the soil-gas flow field is more spread out (Figs. 4 and 5).

The dramatic effect of a subslab gravel layer on soil-gas entry rate can be understood by comparing the measured pressure coupling in the subslab region underneath both structures, as shown in Fig. 3. The pressure coupling of 0.96 measured in the two 0.24-m-long subslab probes underneath the gravel structure reveals that the pressure in the gravel layer is essentially the same as the pressure inside the structure, and that the pressure gradient in the gravel immediately underneath the structure is relatively small. Although the soil-gas flow converges into the bottom of the slots, the small pressure gradient underneath the gravel structure indicates that the gravel presents negligible resistance to soil-gas flow in comparison to the much-lower-permeability native soil. Consequently the gravel layer creates a depressurized plenum underneath the structure which draws radon-laden soil gas into the structure as if the structure had a dirt floor. In contrast, the relatively small value of pressure coupling measured in the two 0.24-m-long probes underneath the no-gravel structure indicates that a large pressure gradient exists immediately underneath the no-gravel structure. The large pressure gradient drives the converging soil-gas flow through the low-permeability native soil and into the bottom of the slots. Model predictions of the pressure coupling field shown in Figs. 6a and 6b support this explanation of the effect of the subslab gravel layer. The relatively flat shape of the 0.9 pressure coupling contour immediately underneath the gravel layer in Fig. 6a indicates that the soil-gas uniformly flows into the gravel layer. In contrast Fig 6b shows the large pressure gradients in the soil near the bottom of the slots.

The performance of the numerical model can be assessed by comparing the model predictions and measurements of pressure coupling around both structures. Figs. 3, 4, and 5 show that the model underpredicts the pressure coupling around both structures at every probe location except the two 2.39-m-long probes in the no-gravel structure low-wall. Around the gravel structure, the model predictions of pressure coupling are more accurate in regions closer to the openings. Fig. 3 shows that the model underpredicts the pressure coupling measured in the 0.24 and 0.5-m-long probes in the subslab of the gravel structure by less than 10%. The accuracy of the model predictions in the region near the gravel layer indicates that the model correctly simulates the effect of a subslab gravel layer. However, the model underpredicts the pressure coupling measured in all of the low-wall probes in the gravel structure by more than a factor of two, and in all of the mid-wall probes by more than a factor of three. In contrast, Figs. 3, 4, and 5 show that the model underpredicts the pressure coupling by at least a factor of two at most probe locations around the no-gravel structure, including the subslab. The general underprediction of the pressure coupling around the no-gravel structure by the model suggests that it does not correctly simulate

the soil-gas pressure field in the critical near slot region. If the model overestimated the pressure drop in the soil near the slots, it would then underpredict the pressure coupling in the rest of the soil block. Such an error could be caused by the value of permeability assigned to the subslab region of the modeled soil block being too small, or an incorrect definition of the interface between the soil and the bottom of the slab. The model assumes that a perfect interface between the soil and the bottom of the slab exists; however, settling could create air gaps under the slab of the no-gravel structure.

Pressure coupling measurements provide details of the soil-gas flow field created by the depressurization of the interior of the structure. The failure of the numerical model to correctly predict the shape of the pressure coupling field indicates that it does not accurately simulate the soil-gas flow field around the structures. Consequently, the factor of 1.5 discrepancy between the measured and modeled soil-gas entry rates into both structures is *not* caused by the permeability measurements used as inputs for the model being a factor of 1.5 too low. Simply increasing the permeability inputs into the model will *not* change the shape of the predicted pressure coupling and soil-gas flow fields. In fact, the comparison of the measurements and model predictions of pressure coupling suggests that the cause of this discrepancy maybe different in each structure.

^{222}*Rn Entry Rate as a Function of Open Area*

Fig. 7 shows the measured and modeled radon entry rate into the structures as a function of open area. The radon entry rates have been normalized by structure depressurization. The measured radon concentration of the air in the openings varied by less than 8% over the entire range of pressures and open areas considered during these experiments; consequently, the radon entry rate can be assumed to vary linearly with structure depressurization. Fig. 7 shows the measured radon entry rate into the gravel structure rapidly increases with open area, reaching a maximum entry rate of approximately 0.8 Bq s^{-1} Pa^{-1} for open areas greater than 5 x 10^{-4} m^2. In contrast, the measured radon entry rate into the no-gravel structure gradually increases with open area. The slightly non-linear response of the measured radon entry rate into the no-gravel structure to changes in open area indicates that there is some coupling between the openings in the floor of the no-gravel structure. However, this response also indicates that a high-permeability region does *not* exist underneath the no-gravel structure. However, during the construction of the no-gravel structure great care was taken to prevent any air gaps or regions of loosely packed soil from forming underneath its slab. Consequently, the results from the no-gravel structure may not be representative of some real houses. Fig. 7 shows that the model accurately predicts the response of radon entry rate into both structures to changes in open area, despite underpredicting the absolute entry rate into both structures by approximately a factor of 1.5. As expected, the model predicts that the radon entry rate into the no-gravel structure will approach the entry rate into the gravel structure as the open area approaches the dirt floor limit, i.e. when no concrete slab is present.

The ratio of radon entry rate into the two structures depends on open area. For the base configuration of six-slots open, Fig. 7 shows that the measured radon entry rate into the gravel structure is four times greater than the entry rate into the no gravel structure -- the same as the ratio of the measured soil-gas entry rates with six slots open. However, with an open area of 5×10^{-4} m^2 the measured radon entry rate into the gravel structure is more than a factor of 30 greater than the entry rate into the no-gravel structure. To significantly reduce the radon entry rate into the gravel structure the open area must be much smaller than 2.5×10^{-4} m^2. This is similar to the results of a field study that concluded that the total open area of a basement must be very small in order to consider it radon resistant (Eaton and Scott 1984).

The spatial distribution of the open area also affects the soil-gas and advective radon entry. The measured soil-gas entry rate through the four 0.013-m-diameter holes into the gravel structure is 30% *higher* than the entry rate through the 0.038-m-diameter hole in the center of the floor despite the four-hole configuration having a total open area more than a factor of 2 *smaller* than the area of the one-hole configuration. Spreading the open area in the floor of the gravel structure reduces the soil-gas velocity in the gravel near the mouth of the opening thus more effectively depressurizing the gravel layer and increasing the total soil-gas and advective radon entry rate. In the no-gravel structure, model predictions of radon entry rate through two opening configurations each with an open area of 110×10^{-4} m^2 were compared: two double-width slots (0.0064 m wide) versus four normal slots (0.0032 m wide). In the four-narrow slot case the predicted radon entry rate into the no-gravel structure was 30% higher than the two-wide slot case. Again distributing the open area to minimize the soil-gas velocities in the soil near the mouth of the openings increased the total soil-gas and advective radon entry rate.

The pressure drop through all of the openings considered in this study is negligible in comparison with the pressure drop in the soil. However, in real structures, the geometry of the opening could result in a significant pressure drop across the slab. In that case the increased resistance of the openings to soil gas flow will reduce the advective radon entry rate; consider for example a rough crack versus a smooth-walled gap.

^{222}*Rn and Soil-gas Entry as a Function of Pressure Coupling*

Our results demonstrate that a complex relationship exists between open area and radon entry rate. Consequently open area is a poor indicator of radon entry potential. Even if the amount of open area can be measured, the radon entry into the structures depends strongly on the presence or absence of a subslab gravel layer as well as the spatial distribution of the open area.

A theoretical relationship between the soil-gas entry rate and the extension of the soil-gas pressure field can be derived using Darcy's law and the principle of conservation of mass. This analysis can be extended to the radon entry rate into the structures because the concentration of slot air was essentially

constant during these experiments. By conservation of mass the flow rate across any surface, S, which extends through the soil underneath the structure connecting the walls and enclosing the floor is equal to the soil-gas entry rate into the structure; an example of such a surface is the 0.1 pressure coupling contour shown around the gravel structure shown in Fig. 6a. Assuming incompressible flow and writing the soil-gas velocity in terms of Darcy's law, the soil-gas entry rate into the structure can be expressed as an integral over the surface S;

$$Q = \int_S \bar{u} \cdot \bar{n} dA = \int_S -\frac{k}{\mu} \nabla P \cdot \bar{n} dA \qquad 5$$

where $\bar{u}$ is the soil-gas velocity, k is the permeability of the soil, μ is the dynamic viscosity of the soil-gas, ∇P is the pressure gradient across the surface S, and $\bar{n}$ is the unit normal vector to surface S. If the surface S is defined such that $k\nabla P \cdot \bar{n}$ is constant and the soil-gas viscosity is constant, then the soil-gas entry rate into the structure can be written as

$$Q = -\frac{k}{\mu} \nabla P \cdot \bar{n} \int_S dA = -\frac{k}{\mu} \nabla P \cdot \bar{n} A \qquad 6$$

where A is the area of surface S. Equation 6 shows that for a given structure depressurization soil-gas entry rate into the structure is proportional to the area of a surface of constant $k\nabla P \cdot \bar{n}$.

Although soil-gas entry rate is proportional to the area of a surface of constant $k\nabla P \cdot \bar{n}$, such a parameter is not a practical predictor of soil-gas entry rate because the calculation of it requires exact knowledge of the soil-gas pressure field. However, the area of a surface of constant $k\nabla P \cdot \bar{n}$ is a measure of the extension of the soil-gas pressure field. The larger the area of such a surface the greater the extension of the pressure field; the greater the extension of the pressure field the larger the region from which the structure draws radon-laden soil gas.

Individual measurements of pressure coupling indicate the extension of the soil-gas pressure field. A comparison of the measured pressure coupling between the two structures is an estimate of the relative extension of their pressure fields. In Fig. 8 the total advective radon entry rate normalized by structure depressurization is plotted as a function of average subslab pressure coupling, which is an average of the pressure coupling measurements made in all of the 0.24, 0.5, and 1.71-m-long subslab probes during each experiment. Pressure coupling measurements from several different probe locations were averaged together to reduce the effect of local soil-heterogeneity on the measure of the extension of the pressure field. The open area of these experiments was varied between 0 and 165 x 10^{-4} m^2. All of the measurements in Fig. 8 in the *gravel structure* with an entry rate less than 0.5 Bq s^{-1} Pa^{-1} were made with imperfectly sealed openings. Initially duct tape and Dux-seal were used to seal the openings in the structures; however, this seal did not eliminate the entry rate through the openings. All of the

measurements in the *no-gravel structure* with an entry rate less than 0.1 Bq s^{-1} Pa^{-1} were made an open area 5.0 x 10^{-4} m^2 or less.

Despite incomplete knowledge of the pressure field, average subslab pressure coupling, an estimate of the extension of the pressure field is a good measure of the radon entry rate into the structures. Fig. 8 shows that the radon entry rate into *both* structures is approximately a linear function of the average subslab pressure coupling regardless of subslab permeability and open area configuration. A linear regression of the radon entry rate into *both* structures as a function of average subslab pressure coupling yields a slope of 1.2 Bq s^{-1} Pa^{-1} per unit of pressure coupling and an intercept of -0.03 Bq s^{-1} Pa^{-1}, $r^2 = 0.97$.

Conclusions

The results of this study demonstrate that a high permeability subslab gravel layer can substantially affect soil-gas and radon entry into houses. The measured radon entry rate into the gravel structure is four times greater than the entry rate into the no-gravel structure with an open area of 165 x 10^{-4} m^2. The ratio of the entry rates into the two structures increases as the open area is reduced; with an open area of 5.0 x 10^{-4} m^2 the entry rate into the gravel structure is factor of 30 greater than the entry rate into the no-gravel structure. The high permeability gravel layer couples the openings in the floor of the gravel structure together, enabling very small open areas to effectively depressurize the gravel layer the same amount as the interior of the structure. Once this occurs the radon entry rate through openings in the floor is maximized. In contrast the openings in the floor of the no-gravel structure act relatively independently of each other. Consequently, an increase in open area in the floor of the no-gravel structures increases the radon entry rate. The impact of a high permeability gravel layer on the soil-gas and radon entry rate underscores the importance of the permeability of the soil near an opening on determining the advective entry through that opening.

The impact of a subslab gravel on radon and soil-gas entry will depend on the permeability of the gravel layer and the surrounding soil. This study only considered the specific combination of soil permeabilities measured at the structure site, see Table 2. However, the results of this study help validate the predictions of numerical models on the effect of different structural and soil parameters on radon and soil-gas entry rate into houses.

Open area is a poor indicator of radon or soil-gas entry rate into the experimental structures. A complex relationship exists between open area and radon and soil-gas entry rate; however the entry rate into the structures depends strongly on subslab permeability, as well as on the amount and distribution of

open area. However, the results of this study demonstrate that the extension of the soil-gas pressure field created by depressurization of the structure interior is an excellent indicator of radon and soil-gas entry into the experimental structures. The radon entry rate into *either* structure had the same linear relationship with average subslab pressure coupling *regardless* of open area or subslab permeability. The average subslab pressure coupling is a measure of the extension of the pressure field. Although a theoretical relationship exists between the extension of soil-gas pressure field and soil-gas entry rate, application of it requires detailed knowledge of the soil-gas pressure field . However the success of the average subslab pressure coupling in capturing the radon entry rate into *both* structures indicates that, even with limited knowledge of the soil-gas pressure field, a crude estimate of its extension provides an excellent indication of the entry potential. In real buildings the extension of the soil-gas pressure field may be a valuable tool for assessing its soil-gas and radon entry potential independent of any physical characteristics of the building.

Comparison of measurements with predictions of a numerical model indicate that a finite-difference model based on Darcy's law with regionally-defined soil parameters accurately simulates the effect of different structure depressurizations, open areas, and subslab permeabilities on radon and soil-gas entry rate. However, the model underpredicts the soil-gas and radon entry rates into both structures by approximately a factor of 1.5. Comparison of the soil-gas pressure fields around both structures suggests that the source of this discrepancy maybe different in each structure. The discrepancy in the case of the gravel structure may be caused by the failure of the model to predict extension of the pressure field around the structure. However, in the case of the no-gravel structure the discrepancy appears to be caused by the model overestimating the pressure drop in the subslab region beneath the structure.

The results of this study also help explain the ineffectiveness of sealing as a radon mitigation technique. In houses with a subslab gravel layer one must seal essentially all of the openings to significantly reduce radon entry. In addition it has implications for building codes which require the inclusion of a subslab gravel layer in high radon areas to facilitate the implementation of an active mitigation system (US EPA 1994). If mitigation measures are not installed or functioning properly the gravel layer can greatly enhance the radon entry rate, potentially increasing indoor radon concentrations.

Acknowledgments -- The authors would like to thank our colleagues W. Fisk, K. Garbesi, R. Greif, and Y. Li for their critical examination of this paper. We are also grateful to the California Department of Forestry and the Ben Lomond Nursery for their hospitality at the field site.

References

Åkerblom, G.; Anderson, P.; Clavensjo, B. Soil gas radon–A source of indoor radon daughters. Radiation Protection Dosimetry 7:49-54; 1984.

Brennan, T. M.; Clarkin, M. E.; Osborne, M. C.; Brodhead, W. P. Evaluation of radon resistant new construction techniques. Proceedings of the 1990 International Symposium on Radon and Radon Reduction Technology. Vol. 2: Atlanta, GA: EPA; EPA-600/9-91-026b; 1991: VIII-1 - VIII-8.

Brimhall, G. H.; Lewis, C. J. Differential element transport in the soil profile at the Ben Lomond small structure radon site: A geochemical mass balance study. Berkeley, CA: Department of Geology and Geophysics, University of California; 1992.

Bruno, R. C. Sources of indoor radon in houses: A review. J. Air. Pollut. Control Assoc. 33:105-109; 1983.

Busigin, A.; van der Vooren, A. W.; Phillips, C. R. Interpretation of the response of continuous radon monitors to transient radon concentrations. Health Phys. 37:659-667; 1979.

Eaton, R. S.; Scott, A. G. Understanding radon transport into houses. Radiat. Prot. Dosim. 7:251-253; 1984.

Fisk, W. J.; Modera, M. P.; Sextro, R. G.; Garbesi, K.; Wollenberg, H. A.; Narasimhan, T. N.; Nuzum, T.; Tsang, Y. W. Radon entry into basements: approach, experimental structures, and instrumentation of the small structures project. Berkeley, CA: Lawrence Berkeley Laboratory; Report LBL-31864; 1992.

Flexser, S.; Wollenberg, H. A.; Smith, A. R. Distribution of radon sources and effects on radon emanation in granitic soil at Ben Lomond, California. Envrion. Geol. 22:162-177; 1993.

Garbesi, K. Toward resolving model-measurement discrepancies of radon entry into houses. Berkeley, CA: Lawrence Berkeley Laboratory; Report LBL-34244; 1993.

Garbesi, K.; Sextro, R. G. Modeling and field evidence of pressure-driven entry of soil gas into a house through permeable below-grade walls. Environ. Sci. Technol. 23:1481-1487; 1989.

Garbesi, K.; Sextro, R. G.; Fisk, W. J.; Modera, M. P.; Revzan, K. L. Soil-gas entry into an experimental basement: Model-measurement comparisons and seasonal effects. Environ. Sci. Technol. 27:466-473; 1993.

Garbesi, K.; Sextro, R. G.; Wooley, J.; Nazaroff, W. W. A field study of the scale dependence of soil permeability to air. Berkeley, CA: Lawrence Berkeley Laboratory; Report LBL-35369; 1994.

Henschel, D. B. Radon reduction techniques for detached houses: Technical guidance (second edition). Research Triangle Park, NC: Air and Energy Engineering Research Laboratory; Report EPA/625/5-87/019; 1988.

Loureiro, C. O.; Abriola, L. M.; Martin, J. E.; Sextro, R. G. Three-dimensional simulation of radon transport into houses with basements under constant negative pressure. Environ. Sci. Technol. 24:1338-1348; 1990.

Modera, M. P.; Bonnefous, Y. Continuous radon monitor multiplexed sampling. Health Phys. 64:291-299; 1993.

Mowris, R. J. Analytical and numerical models for estimating the effect of exhaust ventilation on radon entry in houses with basements or crawl spaces. Berkeley, CA: Lawrence Berkeley Laboratory; Report LBL-22067; 1986.

Mowris, R. J.; Fisk, W. J. Modeling the effects of exhaust ventilation on ^{222}Rn entry rates and indoor ^{222}Rn concentrations. Health Phys. 54:491-501; 1988.

Nazaroff, W. W.; Feustel, H.; Nero, A. V.; Revzan, K. L.; Grimsrud, D. T.; Essling, M. A.; Toohey, R. E. Radon transport into a detached one-story house with a basement. Atmos. Environ. 19:31-43; 1985.

Nazaroff, W. W.; Lewis, S. R.; Doyle, S. M.; Moed, B. A.; Nero, A. V. Experiments on pollutant transport from soil into residential basements by pressure-driven airflow. Environ. Sci. Technol. 21:459-466; 1987.

Nazaroff, W. W.; Moed, B. A.; Sextro, R. G. Soil as a source of indoor radon: Generation, migration, and entry. In: Nazaroff, W. W.; Nero, A. V. eds. Radon and Its Decay Products in Indoor Air. New York: John Wiley and Sons; 1988:57-112.

Nero, A. V.; Nazaroff, W. W. Characterizing the source of radon indoors. Radiat. Prot. Dosim. 7:23-39; 1984.

Revzan, K.; Fisk, W. Modeling radon entry into houses with basements: The influence of structural factors. Indoor Air 2:40-48; 1992.

Rogers, V. C.; Nielson, K. K. Data and models for radon transport through concrete. Proceedings of the 1992 International Symposium on Radon and Radon Reduction Technology. Vol. 2: Minneapolis, MN: EPA; 1992.

Ruppersberger, J. S. The use of coatings and block specification to reduce radon inflow through block basement walls. Proceedings of the 1990 International Symposium on Radon and Radon Reduction Technology. Vol. 2: Atlanta, GA: EPA; EPA-600/9-91-026b; 1991: 8-51.

Scott, A. G. Preventing radon entry. In: Nazaroff, W. W.; Nero, A. V. eds. Radon and Its Decay Products in Indoor Air. New York, N.Y.: John Wiley and Sons; 1988:407-433.

Shah, R. K. A correlation for the laminar hydrodynamic entry length solutions for circular and noncircular ducts. J. Fluid Eng. 100:177-179; 1978.

Thomas, J. W.; Countess, R. J. Continuous radon monitor. Health Phys. 36:734-738; 1979.

Turk, B. H.; Harrison, J.; Sextro, R. G. Performance of radon control systems. Energy Build. 17:157-175; 1991a.

Turk, B. H.; Prill, R. J.; Fisk, W. J.; Grimsrud, D. T.; Sextro, R. G. Effectiveness of radon control techniques in fifteen homes. J. Air Waste Mange. Assoc. 41:723-734; 1991b.

Turk, B. H.; Prill, R. J.; Grimsrud, D. R.; Moed, B. A.; Sextro, R. G. Characterizing the occurrence, sources and variability of radon in Pacific Northwest homes. J. Air Waste Mange. Assoc. 40:498-506; 1990.

U.S. Environmental Protection Agency. Model standards and techniques for control of radon in new residential buildings. Federal Register Notices 59:13402-13416; 1994.

Table 1. Location of soil probes around both structures. As shown in Fig. 1, high-wall, mid-wall, and low-wall probes extend horizontally from the walls at the specified depth, and subslab probes extend vertically through the slab of each structure. Probe length is measured from the outside of wall or floor slab to the middle of the sampling screen. The labels N,S,E,W identify one horizontal probe and the wall from which it extends -- North, South, East, or West.

		Probe Length (m)				
		0.24	0.5	1.11	1.71	2.39
Level Name	Depth Below Grade (m)	Number and Location of Probes				
High-wall	0.2	0	N,S,E,W	0	E,W	N,S
Mid-wall	0.8	0	N,S,E,W	0	E,W	N,S
Low-wall	1.6	0	N,S,E,W	0	E,W	N,S
Subslab (No-Gravel)	2	2	2	2	2	0
Subslab (Gravel)	2	2	2	0	3	1

Table 2. Measured soil and gravel permeability at structure site.

Soil Type	Horizontal Permeability (m^2)	Vertical Permeability (m^2)
undisturbed[a]	3.0×10^{-11}	1.8×10^{-11}
backfill[b]	3.5×10^{-12}	3.5×10^{-12}
gravel[c]	2.0×10^{-8}	2.0×10^{-8}

[a](Garbesi 1993; Garbesi et al. 1994)
[b](Garbesi et al. 1993)
[c](Fisk et al. 1992)

Table 3. Measured soil properties at structure site.

Depth of Layer (m)	Soil-grain Density[a] ($kg\ m^{-3}$)	Radium Content[b] ($Bq\ kg^{-3}$)	Air-filled Porosity[a]	Emanation Fraction[b]
0 - 1.4	2.80×10^3	30	0.45	0.31
1.4 - 2.25	2.80×10^3	30	0.45	0.45
2.25 - 6	2.80×10^3	30	0.25	0.31

[a](Brimhall and Lewis 1992)
[b](Flexser et al. 1993)

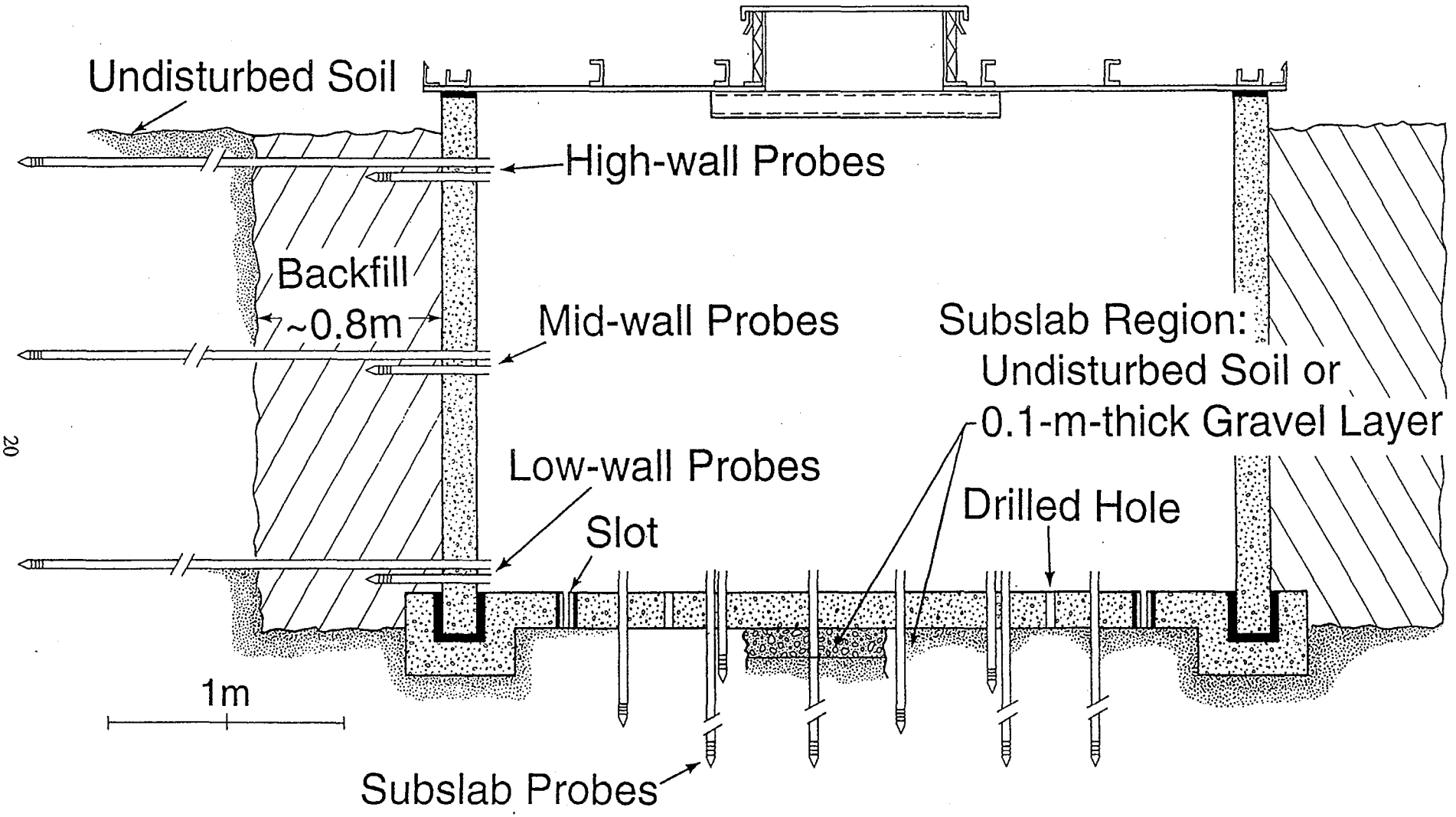

Fig. 1. Schematic diagram of north-south cross section of the experimental structures. Soil probes extend from all four walls of the structure, but are omitted for visual clarity

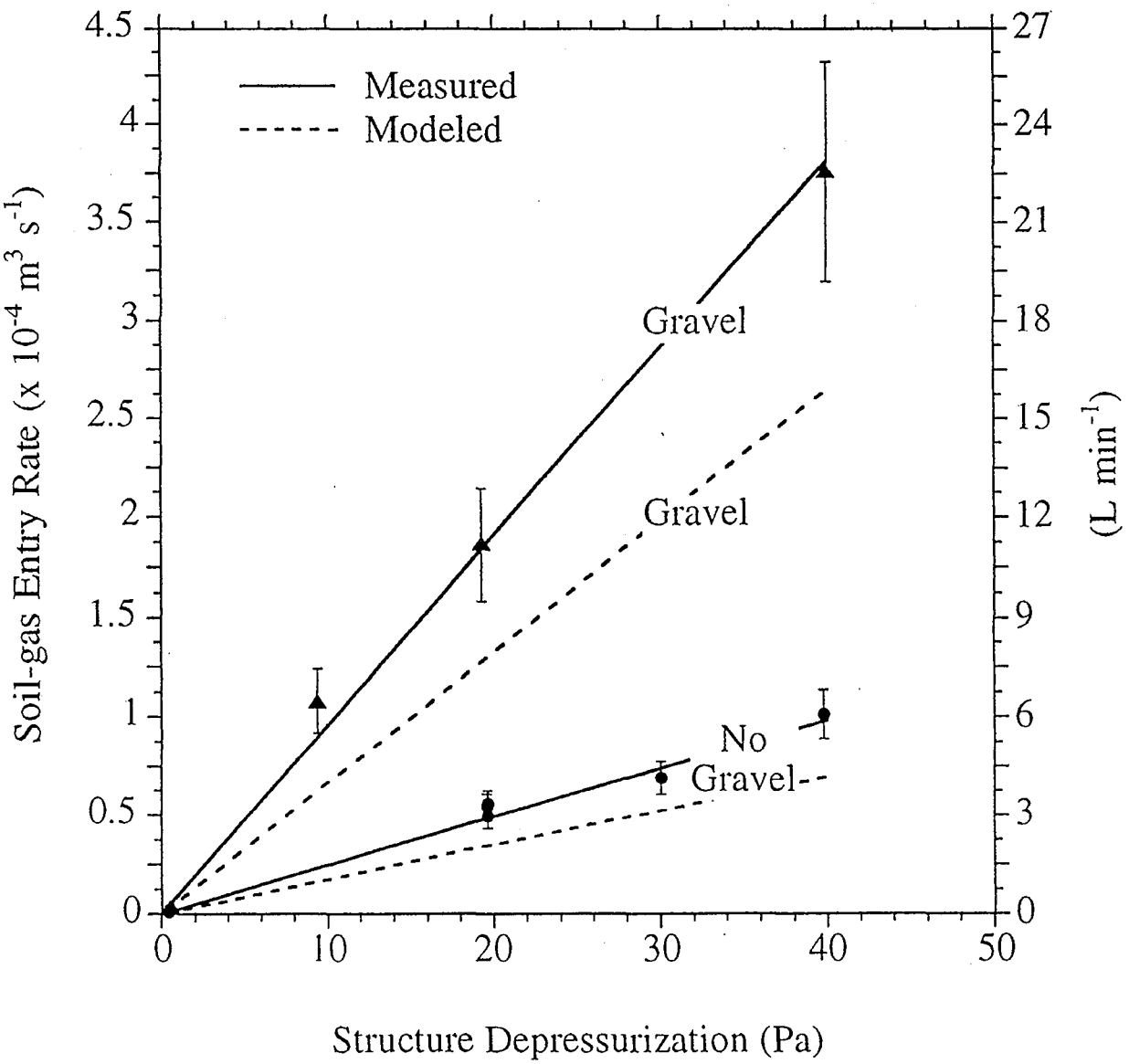

Fig. 2. A comparison of measured and modeled soil-gas entry rate into both structures as a function of structure depressurization. Lines through measured points are linear regressions weighted by uncertainties. The vertical bars represent measurement uncertainty.

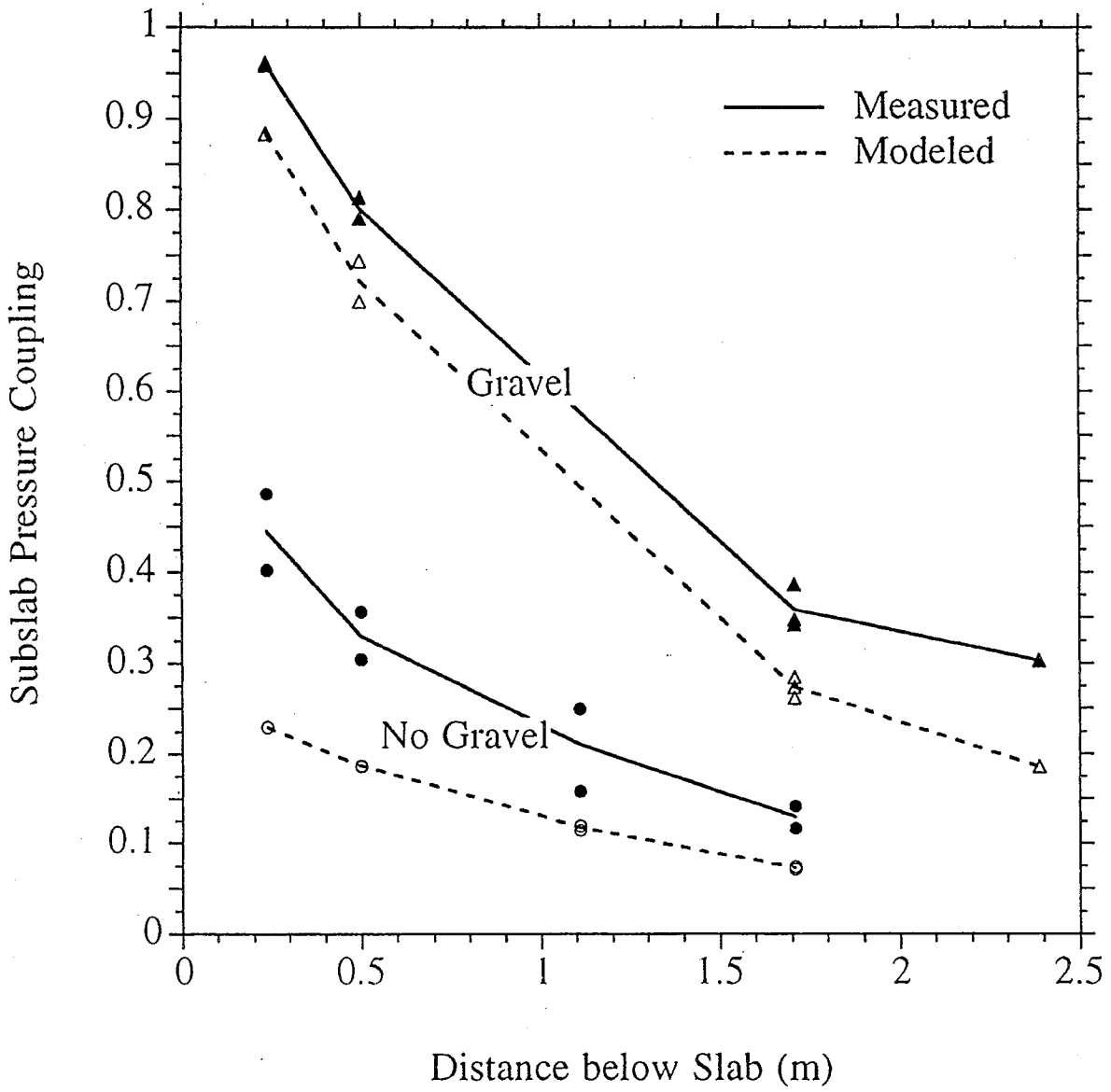

Fig. 3. A comparison of measured and modeled subslab pressure coupling underneath both structures with all six slots open. Lines connect average values for a each probe length and are intended for visual guidance only. Note there are no 1.11-m-long probes underneath the gravel structure, and no 2.39-m-long probes underneath the no-gravel structure. Measured values indicated by solid symbols; modeled values indicated by open symbols. The maximum uncertainty on the measurements is ±0.02 in the no-gravel structure, and ±0.03 in the gravel structure.

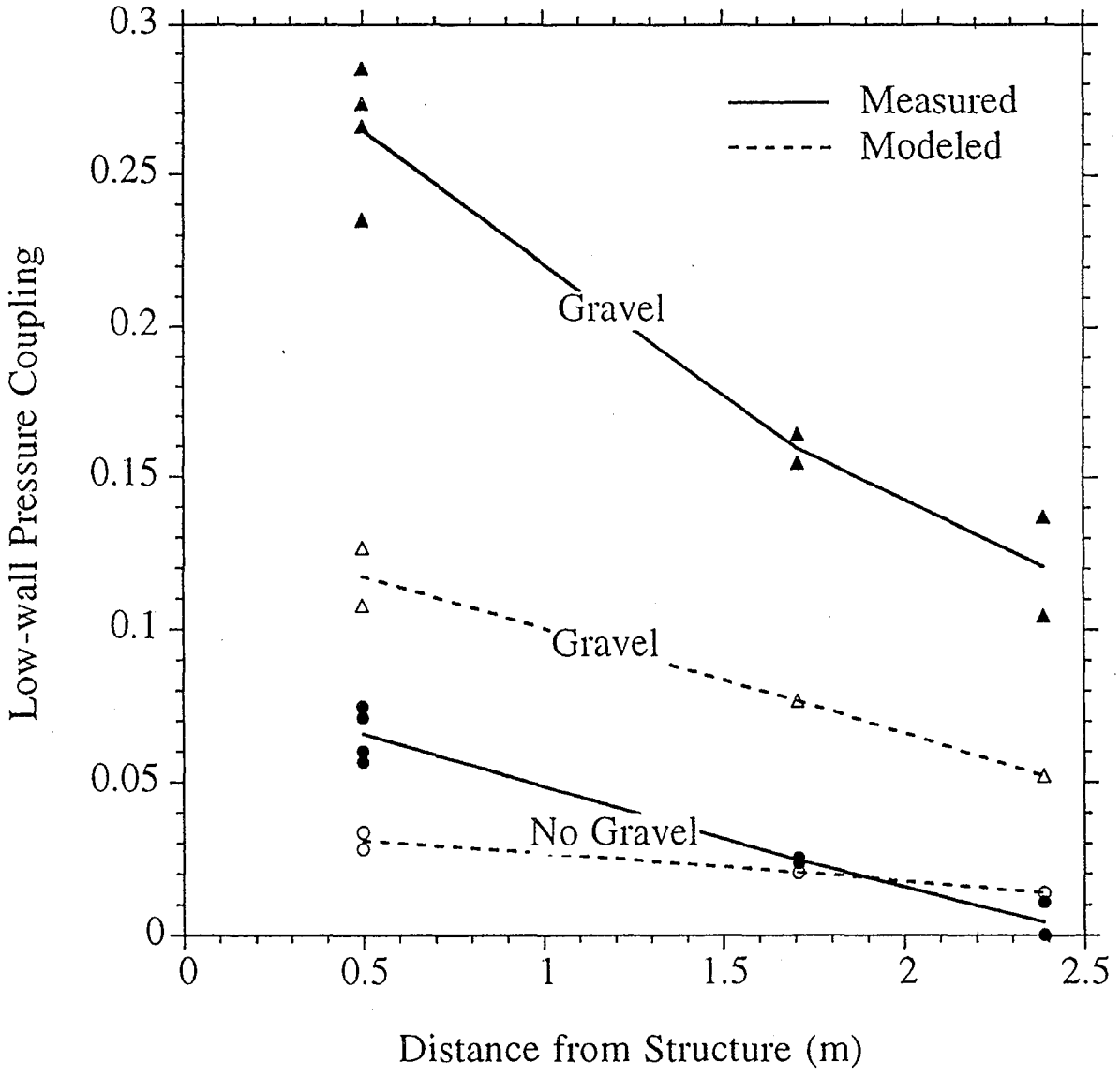

Fig. 4. A comparison of measured and modeled low-wall (1.6 m below grade) pressure coupling around both structures with all six slots open. Lines, symbols, and uncertainties are the same as in Fig. 3.

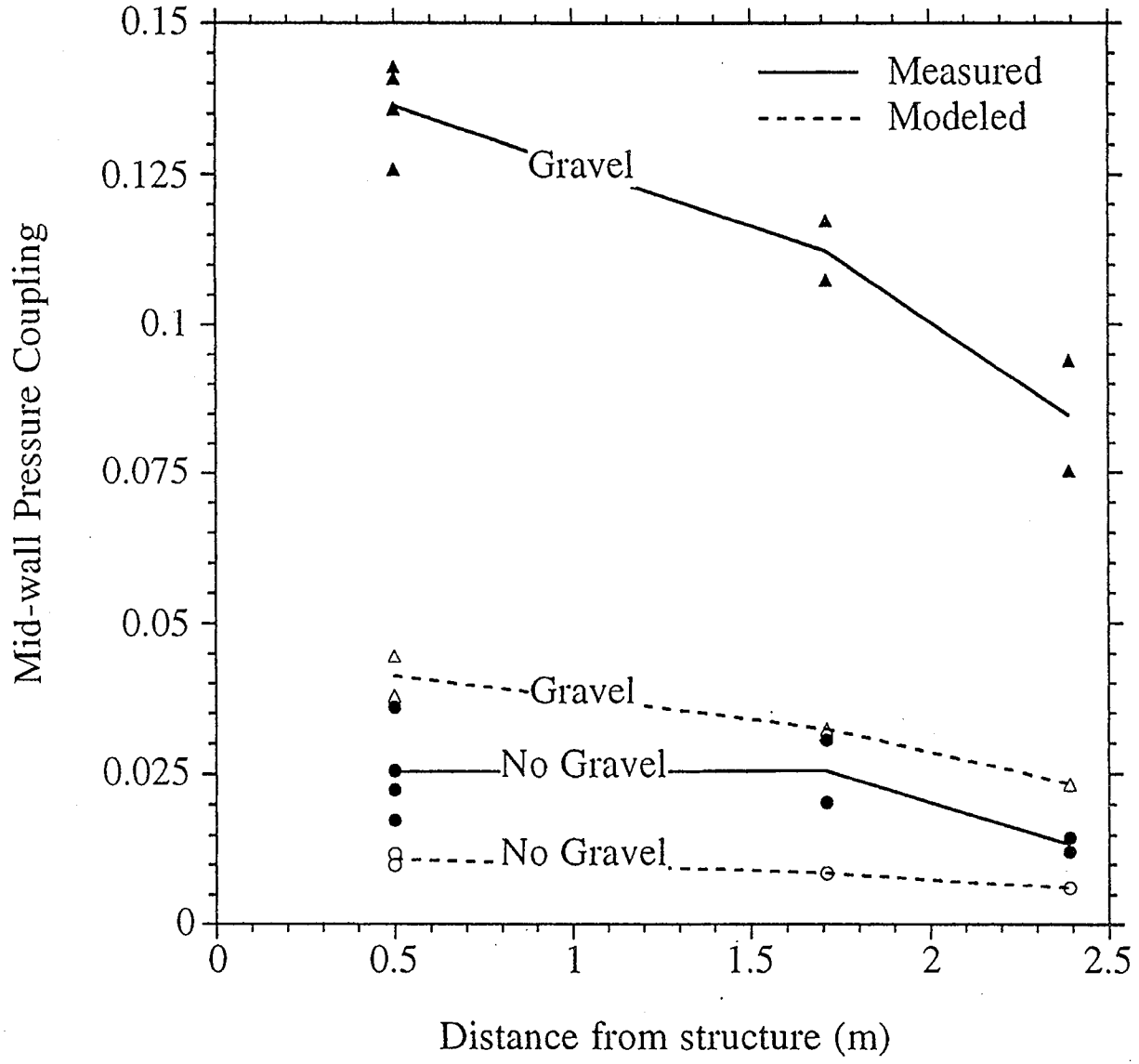

Fig. 5. A comparison of measured and modeled mid-wall (0.8 m below grade) pressure coupling around both structures with all six slots open. Lines, symbols, and uncertainties are the same as in Fig. 3.

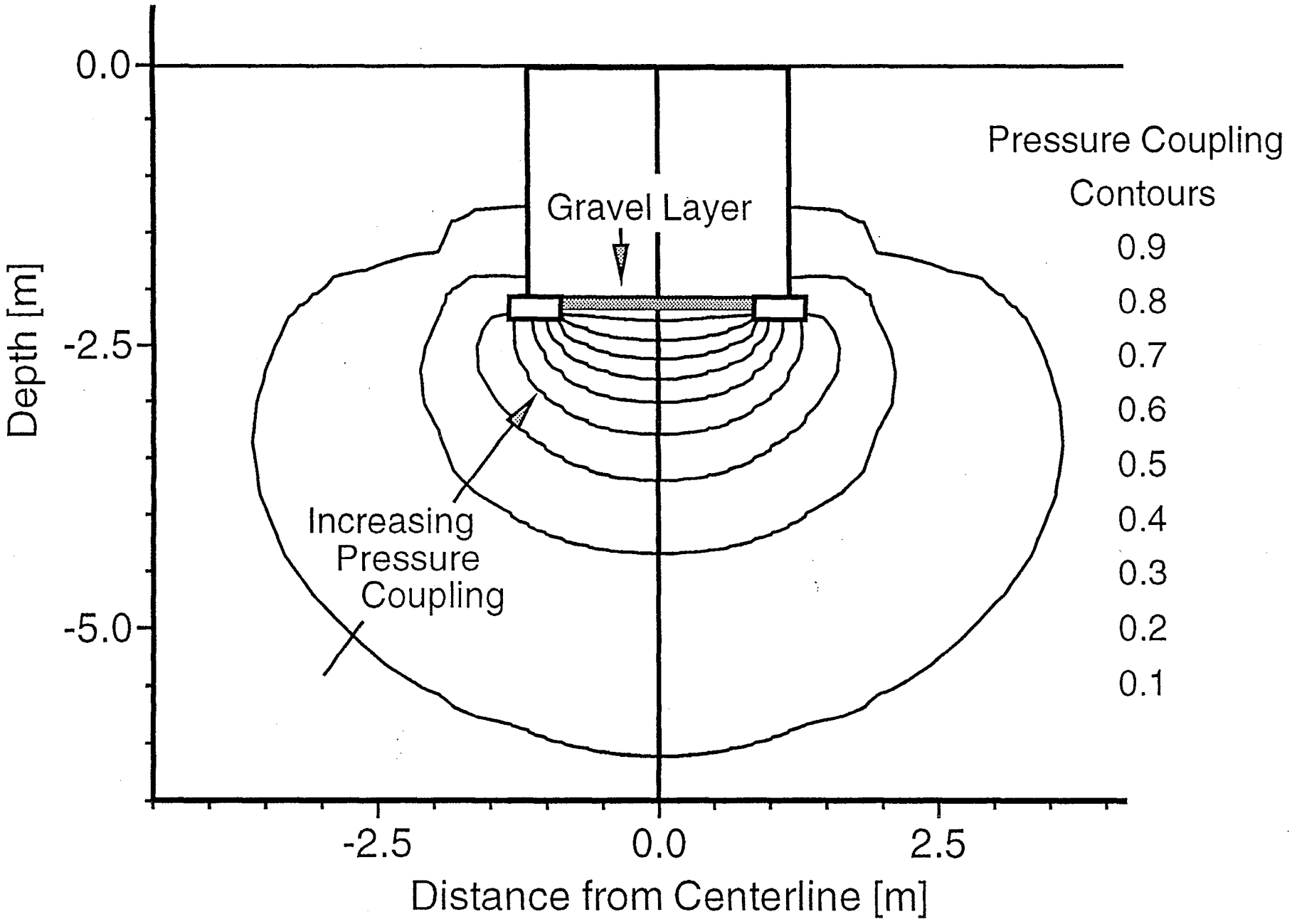

Fig. 6a. Model prediction of the pressure coupling field in the east-west cross-section around the gravel structure with all six-slots open. Lines are pressure coupling contours. The line down center of the figure represents the model's plane of symmetry.

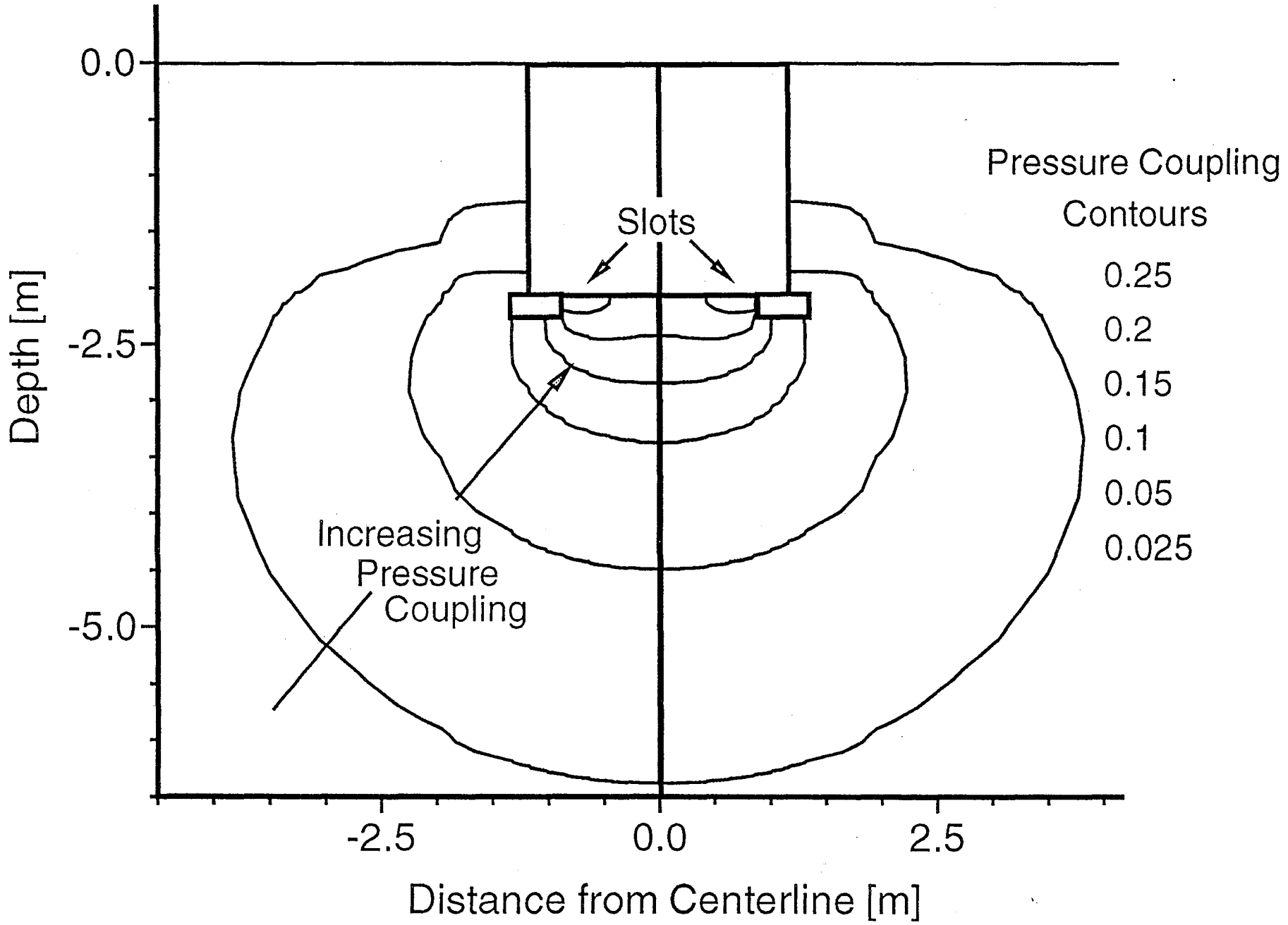

Fig. 6b. Model prediction of the pressure coupling field in the east-west cross-section around the no-gravel structure with all six-slots open. Lines are pressure coupling contours. The line down center of the figure represents the model's plane of symmetry.

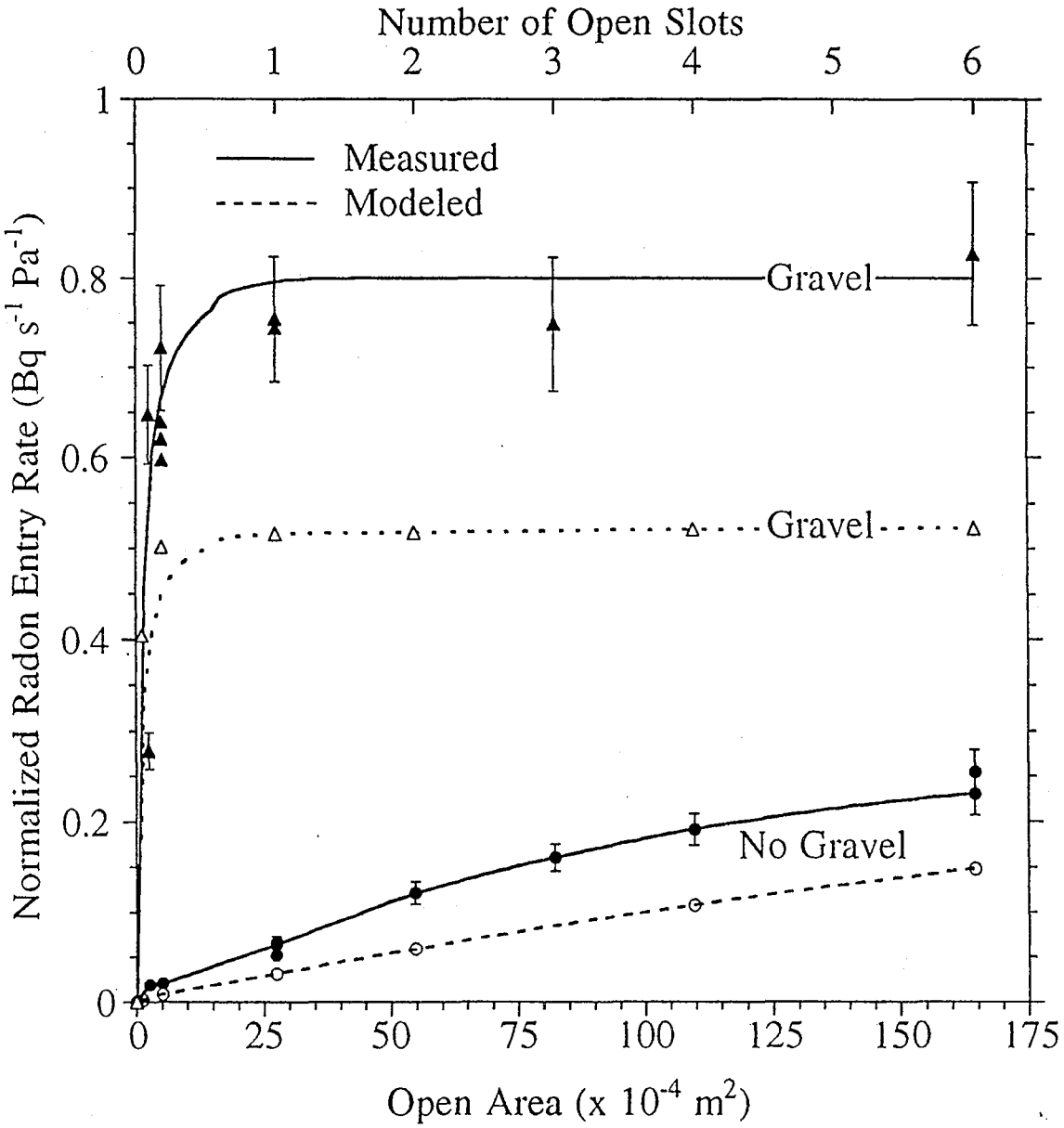

Fig. 7. A comparison of measured and modeled advective radon entry rate normalized by structure depressurization as a function of open area. Solid symbols indicated measured values; open symbols indicate modeled values. Lines are intended for visual guidance only. The vertical bars represent experimental uncertainty.

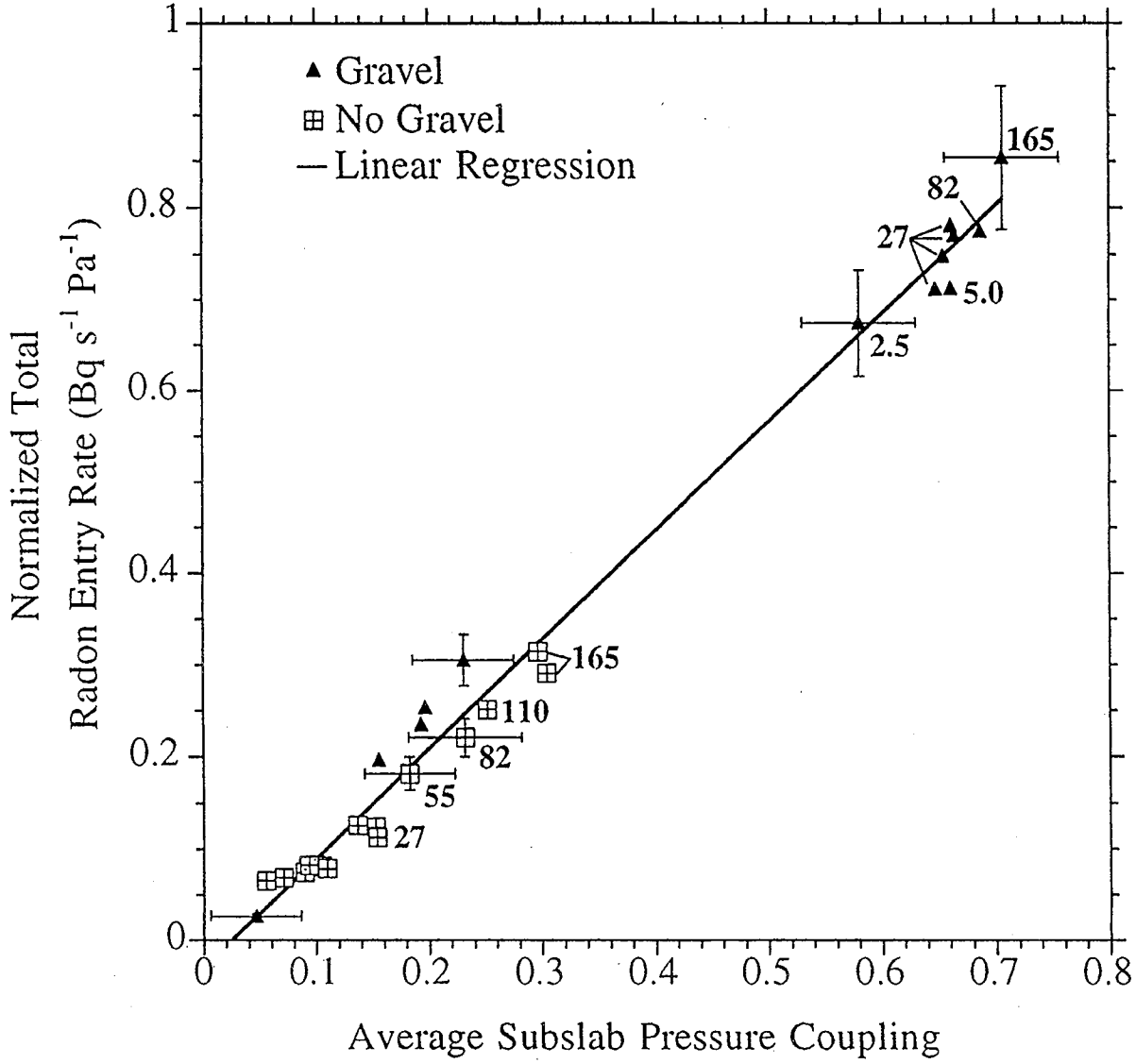

Fig. 8 Measured total advective radon entry rate into both structures normalized by structure depressurization as a function of average subslab pressure coupling. Numbers indicate open area in units of 10^{-4} m^2. Vertical bars indicate uncertainty of measured radon entry rate, a maximum of 12%; horizontal bars indicate uncertainty of average pressure coupling, a maximum of ±0.05. Error bars omitted on some points for visual clarity.